Hindawi
Geofluids
Volume 2019, Article ID 4363592, 20 pages
https://doi.org/10.1155/2019/4363592

Research Article

A Review of the Hydrochemistry of a Deep Sedimentary Aquifer and Its Consequences for Geothermal Operation: Klaipeda, Lithuania

Maren Brehme,[1] **Kerstin Nowak**,[2] **David Banks**,[3] **Sigitas Petrauskas**,[4] **Robertas Valickas**,[4] **Klaus Bauer**,[1] **Neil Burnside**,[3] **and Adrian Boyce**[5]

[1]*Deutsches GeoForschungsZentrum (GFZ), Telegrafenberg, D-14473 Potsdam, Germany*
[2]*Geothermie Neubrandenburg GmbH, Seestrasse 7A, D-17033 Neubrandenburg, Germany*
[3]*School of Engineering, James Watt Building (South), Glasgow University, Glasgow G12 8QQ, UK*
[4]*UAB "Geoterma", Lypkių gatvė 17, LT-94100 Klaipėda, Lithuania*
[5]*Scottish Universities Environmental Research Centre, Rankine Avenue, Scottish Enterprise Technology Park, East Kilbride G75 0QF, UK*

Correspondence should be addressed to Maren Brehme; brehme@gfz-potsdam.de

Received 26 September 2018; Accepted 9 January 2019; Published 9 April 2019

Academic Editor: Julie K. Pearce

The Klaipeda Geothermal Demonstration Plant (KGDP), Lithuania, exploits a hypersaline sodium-chloride (salinity c. 90 g/L) groundwater from a 1100 m deep Devonian sandstone/siltstone reservoir. The hydrogen and oxygen stable isotope composition is relatively undepleted ($\delta^{18}O$ = c. -4.5‰), while the $\delta^{34}S$ is relatively "heavy" at +18.9‰. Hydrochemical and isotopic data support the existing hypothesis that the groundwater is dominated by a hypersaline brine derived from evapoconcentrated seawater, modified by water-rock interaction and admixed with smaller quantities of more recent glacial meltwater and/or interglacial recharge. The injectivity of the two injection boreholes has declined dramatically during the operational lifetime of the KGDP. Initially, precipitation of crystalline gypsum led to a program of rehabilitation and the introduction of sodium polyphosphonate dosing of the abstracted brine, which has prevented visible gypsum precipitation but has failed to halt the injectivity decline. While physical or bacteriological causes of clogging are plausible, evidence suggests that chemical causes cannot be excluded. Gypsum and barite precipitation could still occur in the formation, as could clogging with iron/manganese oxyhydroxides. One can also speculate that inhibitor dosing could cause clogging of pore throats with needles of calcium polyphosphonate precipitate.

1. Introduction

The small country (65,000 km^2) of Lithuania contains a varied geological sequence [1], comprising a largely continental or epicontinental sedimentary sequence, which dips and thickens towards the north-west, overlying metamorphic and metasedimentary "basement" rocks of the Precambrian Baltic Shield. At the coast of the Baltic, the sedimentary cover exceeds 2.3 km in thickness [2], and around Klaipeda, the "basement" comprises varying metasedimentary, metavolcanic rocks, including granulite facies gneisses and migmatites [3]. The country is almost entirely dependent on groundwater, sourced from ca. 20 sedimentary aquifer horizons [3].

1.1. Geothermal Resources of Lithuania. According to [3], the groundwater temperature in the Vydmantai experimental borehole (55°53′42″N 21°08′09″E), which was 2.56 km deep and encountered the top of the Precambrian basement (tuffs, schists, charnockite, gneiss, and granite-gneiss) at 2.12 km deep, reached 90°C (Figure 1—an average geothermal gradient of 0.035 $K\,m^{-1}$), although another source cites a slightly lower temperature (83.6°C) and geothermal gradient, together with a heat flow density of 55 $mW\,m^{-2}$ [4]. In

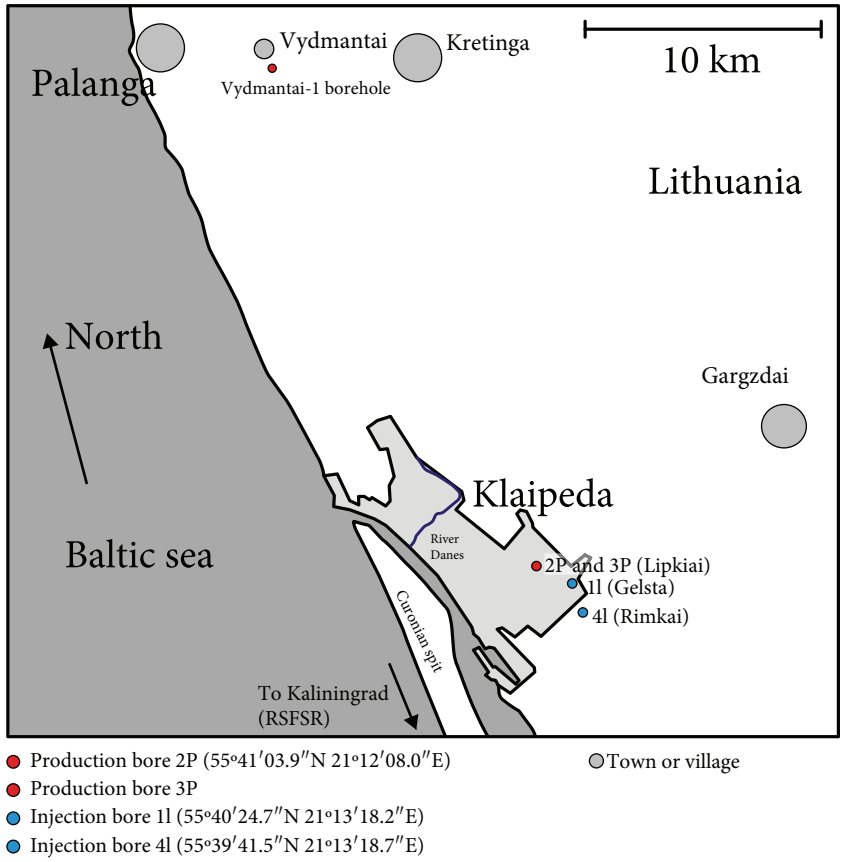

Figure 1: Map of coastal Lithuania, showing the locations of Palanga, Klaipeda, the Vydmantai borehole, and the Klaipeda Geothermal Demonstration Project (KGDP), consisting of boreholes 1I, 2P, 3P, and 4I.

groundwater in the crystalline basement in the core of the Baltic Synclinorium in Western Lithuania, the total mineralisations of 140-200 g L^{-1} are reported (Table 1), compared with standard seawater at 35 g L^{-1}.

Potential "wet" geothermal resources (i.e., hot sedimentary aquifers) have been identified [2] at three stratigraphic horizons in Lithuania:

(i) Upper-Middle Devonian (Šventoji (D_3)-Upninkai (D_2)) complex

(ii) Middle-Lower Devonian (D_2-D_1) complex (Parnu-Kemeri-Gargždai series)

(iii) Cambrian (Deimena-Kybartai-Gegė-Virbalis strata)

The western region of Lithuania, around Klaipeda, has long been recognised as the most promising area for geothermal resources with geothermal gradients exceeding 0.035 K m^{-1} and geothermal heat fluxes of up to 108 m W m^{-2} [5, 6].

The Upper Devonian (D_3-D_2) complex comprises the Šventoji and Upninkai units, which are composed of sands and poorly cemented sandstones, silts, clays, and some dolomitic marls. According to [2], boreholes drilled 300-400 m deep into the D_3 aquifer system of Jūratė and Kastytis, near Palanga (c. 30 km north of Klaipeda), yielded mineral waters of temperature 15°C, of total mineralisation c. 3.2 g L^{-1}, and dominated by Ca-(Mg)-SO_4 in terms of their major ion chemistry. In the same (Palanga) area, slightly deeper boreholes at Eglė, Naglis, Palanga, and Žilvinas (450-680 m) into D_2-D_3 (Šventoji-Upninkai formations) strata yielded much more highly mineralised (12-34 g L^{-1}) and warmer (16-18°C) waters of Na-Cl composition, with the proportion of chloride, temperature, and the total mineralisation increasing with depth.

Summaries of the lithology of the Middle-Lower Devonian (D_2-D_1) complex are provided by [2, 5]. The Parnu sandstones, uppermost in the complex, are typically 20-40 m thick and comprise gypsiferous sandstone interbedded with siltstone, clay, and dolomitic marl. The Kemeri Series comprises laminated fine-grained sandstones with silt and clay. Within the Kemeri Series, the Viešvilė (clay-dominated) strata comprise c. 35 m and the Šešuvis (sandstone-dominated) strata around 100 m. The lowermost Gargždai Series is composed of clays, clayey silt, silts, and sandstones. The facies is continental, although it becomes progressively more distal (fine-grained and clayey) towards the west. Individual Kemeri sandstone units can be up to 14 m thick with a sand content of 70-80%, porosities of 15-25%, and permeabilities of several 100 to 1000s of mD. Groundwater mineralisation in the Kemeri strata can reach up to 85 g/L [2], with

Table 1: Reported range of compositions of groundwater brines in the Precambrian basement in the centre of the Baltic Synclinorium in Western Lithuania [3].

Cations	Concentration ($g\,L^{-1}$)	Anions	Concentration ($g\,L^{-1}$)
Na^+	30-40	Cl^-	100-200
Ca^{2+}	20-30	HCO_3^-	10-30
Mg^{2+}	3-4	$SO_4^=$	0.03-0.4
K^+	0.7-0.9	Br^-	0.7-1.2
Sr^{2+}	0.3-0.4	I^-	0.002-0.004
NH_4^+	0.02-0.1		
Fe^{2+}	0.1-0.5		
Li^+	0.009-0.010		

groundwater being dominated by sodium and chloride but with a Na/Cl ratio < 1.

The Cambrian complex also comprises a series of quartz sandstones, silts, and argillites.

1.2. Geothermal Exploration and the Klaipeda Geothermal Demonstration Plant (KGDP). By 1988, Professor J. Dyadkin had documented the potential of geothermal energy for urban heat supply; by 1990, detailed plans had been worked out for geothermal exploitation in Palanga, and in 1991, the "Geoterma" enterprise had been established to implement these plans [2].

In the 1990s, the Vydmantai borehole was constructed to over 2 km depth into the Precambrian basement. It was eventually decided that the Cambrian geothermal complex was the most promising resource to exploit in order to heat a greenhouse complex [2] using a well doublet. The temperature of the Cambrian hydrothermal complex was around 73°C in a depth interval of 1972 to 2123 m, with the water having a mineralisation of $164\,g\,L^{-1}$ [4].

The Klaipeda Geothermal Demonstration Project (KGDP—Figure 1), which is the subject of this paper, targets the middle D_2-D_1 geothermal stratigraphic complex—specifically the lower Devonian (D_1) Kemeri sandstones (Figure 1). The construction of the KGDP was financed [7] by the Danish Environmental Protection Agency, the Government of Lithuania, the World Bank (IBRD), the EU PHARE programme, and the Global Environmental Facility Trust Fund, with a total budget of 19.5 million USD [8]. The plant is located a short distance SE of the city centre, within the city's free economic zone. Drilling of the four main boreholes, two productions (2P and 3P) and two injections (1I and 4I), was carried out in 1997-98, while geothermal heat production started in earnest in 2000-2001. A history of activities of the site is documented by GTN [9].

The two abstraction wells at KGDP are a little over 1100 m deep. Initial reservoir temperatures and salinities of 38°C and 93 g/L, respectively, were recorded [10], with borehole yields of 300-400 m^3/h (83–111L/s) being typical. The scheme was envisaged as producing 700-800 m^3/h in total from two production boreholes (2P and 3P) at the main site at Lypkiai, using downhole submersible pumps. The produced water entered an array of LiBr absorption heat pumps at c. 36°C. Heat was extracted from the geothermal water, which was then to be reinjected at around 11°C and 24-40 bar, using injection pumps, at boreholes 1I (at Gelsta) and 4I (at Rimkai). The heat pumps were powered by gas boilers, supplying hot water to the heat pumps at 175°C (return 130°C). The heat pumps supplied the district heating network at a design temperature of 70°C (return 40°C [10]). The initial projected peak heat delivery was 49 MW_{th} and 598 TJ/year (25% of Klaipeda's heat demand). The real figure achieved was closer to 41 MW_{th}, of which 24 MW_{th} was ultimately derived from gas combustion and 17 MW_{th} from the geothermal water (an effective coefficient of performance of 1.7). By 2004, some 233,000 MWh (839 TJ) had been produced for district heating in the city of Klaipeda.

Borehole 3P has since been decommissioned, partly due to it producing heavily gypsum-saturated brine (which led to plugging up pipework with gypsum) and partly due to reduced injectivity in the reinjection wells placing a limit on the overall quantity of water that could be produced and reinjected (in reality, some 200 m^3/h). The site supplied a district heating network to numerous clients, although since 2013, it only operated from October to April. In 2017, the KGDP was shut down, ostensibly as it could not compete with a nearby waste-incineration plant in terms of economic supply of heat to the district heat network (although reduced injectivity in 1I and 4I could be cited as a contributory factor [11]).

1.3. Anticipated Geology. The Lower Devonian sandstone reservoir accessed by the KGDP is described [10] on the basis of the core obtained from the Vydmantai borehole. The strata are composed of alternating sandstone and clayey units, with the sandstone units being of 2–18 m thick and accounting for some 70% of the total thickness. The sandstones are described as light grey to grey, of varying grain size, dominated by quartz (69-95%), with subsidiary feldspar (3.2 to 6.4%, occasionally up to 16.4%), and variably micaceous (0.4-1%, occasionally up to 9.4%). Glauconitic sandy and silty horizons sometimes occur, and the sandstones are typically weakly cemented by a clayey or dolomitic matrix. Recorded permeabilities vary from 207 to 6295 mD (average 2563 mD) and open porosities from 20.1 to 31.2% (average 25%) [10]. A transmissivity of c. 150 Dm was anticipated at Klaipeda.

Table 2 documents the mineralogies identified by XRD analyses of white-grey to reddish core samples from the stratigraphic depth of the Klaipeda geothermal reservoir. The main component of all rock types is quartz. The sandstones contain also dolomite, biotite, orthoclase, manganese sulphide (MnS), and kaolinite. Kaolinite is also a major component of the claystones, alongside illite, muscovite, chlorite, and calcite. Siltstones have additionally been observed to contain magnetite.

1.4. Well Construction. Well 2P was constructed in 1997 to 1123 m bgl (1116 m bsl), with the Kemeri sandstones being encountered between 985 and 1113 m bgl (Figure 2); these are described as light grey, fine-medium-grained sandstones with some silt and clay and with some gypsum in the lower

Table 2: Minerals identified (by X-ray diffraction) in core material recovered from reservoir depth in the Klaipeda 1I sidetrack (samples designated KLA1I) and from the deep boreholes Palanga-318 (PAL) and Vydmantai-1 (VID). The figures forming the latter part of the sample number indicate depths in m.

(a)

Core sample Lithology	KLA 1I A	KLA 1I B	PAL 875 Red-grey sandstone	PAL 896.5 Reddish clay	PAL 936 Reddish-grey sandstone	PAL 970 Grey siltstone	PAL 975.5 Grey-red sandstone	PAL 990 Grey-green sandstone	VID 903.3 Grey-white clay
Minerals	Calcite	Quartz	Quartz	Quartz	Quartz	Quartz	Quartz	Quartz	Quartz
	Pyrite	Dolomite	MnS	Muscovite	MnS	Magnetite	MnS	Dolomite	Biotite
	MnS	Calcite		Biotite		MnS	Calcite	MnS	Kaolinite
	Orthoclase			Kaolinite		Kaolinite		Kaolinite	MnS
	Quartz			MnS		Biotite			
				Hematite		Illite			

(b)

Core sample Lithology	VID 913.5 Grey-green clay	VID 944.9 White clay	VID 954.4 Grey clay	VID 958.5 Grey-green clay	VID 962.5 Reddish clay	VID 964 Reddish clay	VID 971 Grey sandstone with clay	VID 972 Grey clay	VID 980 White clay
Minerals	Quartz	Quartz	Quartz	Quartz	Quartz	Quartz	Quartz	Quartz	Quartz
	Illite	Calcite	Biotite	Kaolinite	Hematite	MnS	Biotite	Biotite	MnS
	Kaolinite	MnS	Kaolinite	Illite	Illite	Illite	Kaolinite	MnS	Kaolinite
	Muscovite		MnS	Biotite	Kaolinite	Chlorite			
	MnS			Chlorite	Chlorite				
					Muscovite				

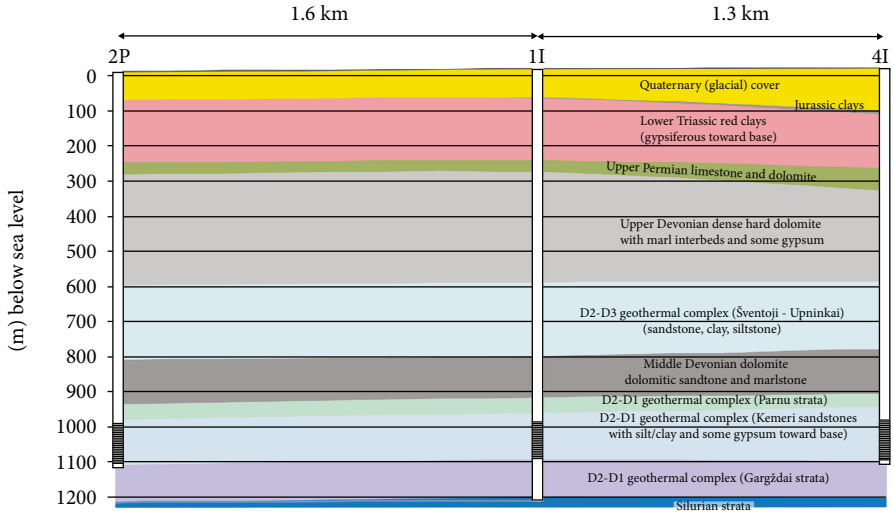

Figure 2: Geological section of Klaipeda geothermal wellfield (as constructed), showing locations of well screens (each screen represented may represent several discrete screened sections within the interval). 2P and 3P are in the NW and 4I in the SE. Based on information in [16] and drilling logs [12–15].

part. The final internal diameters were nominal 13″ casing to 441 m bgl, with 9 5/8″ casing from 335 to 995 m bgl. A final hanging string of nominal 7″ K55 carbon steel casing and screen actual 6.45″ internal diameter was installed from 920 m bgl, with three sections of 0.008″ (0.2 mm) mesh screen (cumulative length c. 93 m) installed opposite the most promising sandstone horizons. The top of the screen was at 998 m bgl, and the base of the lowest screen section was 1110 m bgl. A 40/60 mesh (0.25 to 0.42 mm) gravel pack was washed into place between the 10 5/8″ annulus outside the 7.44″ OD screen [12, 13].

The injection wells 1I and 4I were very similarly constructed (same screen and gravel pack types) with the exception that the diameters were slightly larger, the final screen and casing string being installed in the Kemeri sandstones at 9 5/8″ nominal diameter, within a 15″ annulus [14, 15]. Test pumping of borehole 4I indicated sandstone permeability of 2.1 to 2.5 mD and a transmissivity potentially as high as 218 Dm [11].

In 2009, as a potential (but ultimately unsuccessful) remedy for declining injectivity, a sidetrack borehole was constructed in borehole 1I at a 3.5° deviation from the vertical between 897 m bgl and 1116 m bgl (total depth). In sandstone core recovered from this sidetrack, a typical porosity of 26% was recorded by mercury porosimetry, and 80% of this pore space was found to have an aperture of between 3 and 40 μm [11].

2. Declining Injectivity

Over time, the injectivity of the boreholes 1I and 4I has declined dramatically, as described in full in [9, 11, 16] and summarised graphically in Figure 3. Numerous methods have been trialled to attempt to reverse the transmissivity decline including

(i) acidisations

(ii) reverse pumping

(iii) bactericides

(iv) radial jet drilling

(v) new sidetrack borehole in 1I (2009)

None of these has produced anything other than short-term gains in injectivity. The most successful remediation was the acidisation of both boreholes in 2002 with 20 m^3 18% hydrochloric acid, but even in this case, the injectivity gains were temporary. The fact that productivity is far higher than injectivity when the injection wells are reverse pumped leads Brehme et al. [11] to suppose that the declining injectivity is due to a "skin effect" relatively close to the borehole, which can be partially "drawn out" by abstraction.

In 2003-04, massive gypsum precipitation from the geothermal brine in surface pipework (to the extent that up to 70% of pipeline diameter was obstructed) caused a plant shutdown for thorough remediation [9, 11]. On restarting the operation, the geothermal production water was dosed at wellhead with the complexing agent Labuxan 206 (a solution of sodium phosphonate) at a rate of 30 litres every 48 hrs [16].

Brehme et al. [11] have already discussed in full the possible causes of injectivity decline. These can be listed as follows.

(i) Mineral Precipitation. Aside from the obvious candidate minerals (sulphates and carbonates), there has been some suggestion that traces of oxygen are entering the otherwise reducing water via surface plant, allowing potential oxidation of dissolved iron and manganese.

(ii) Particulate Matter. Monitoring has detected particles of aquifer minerals (sand and clay) which are being drawn in through the gravel pack (250-420 μm)

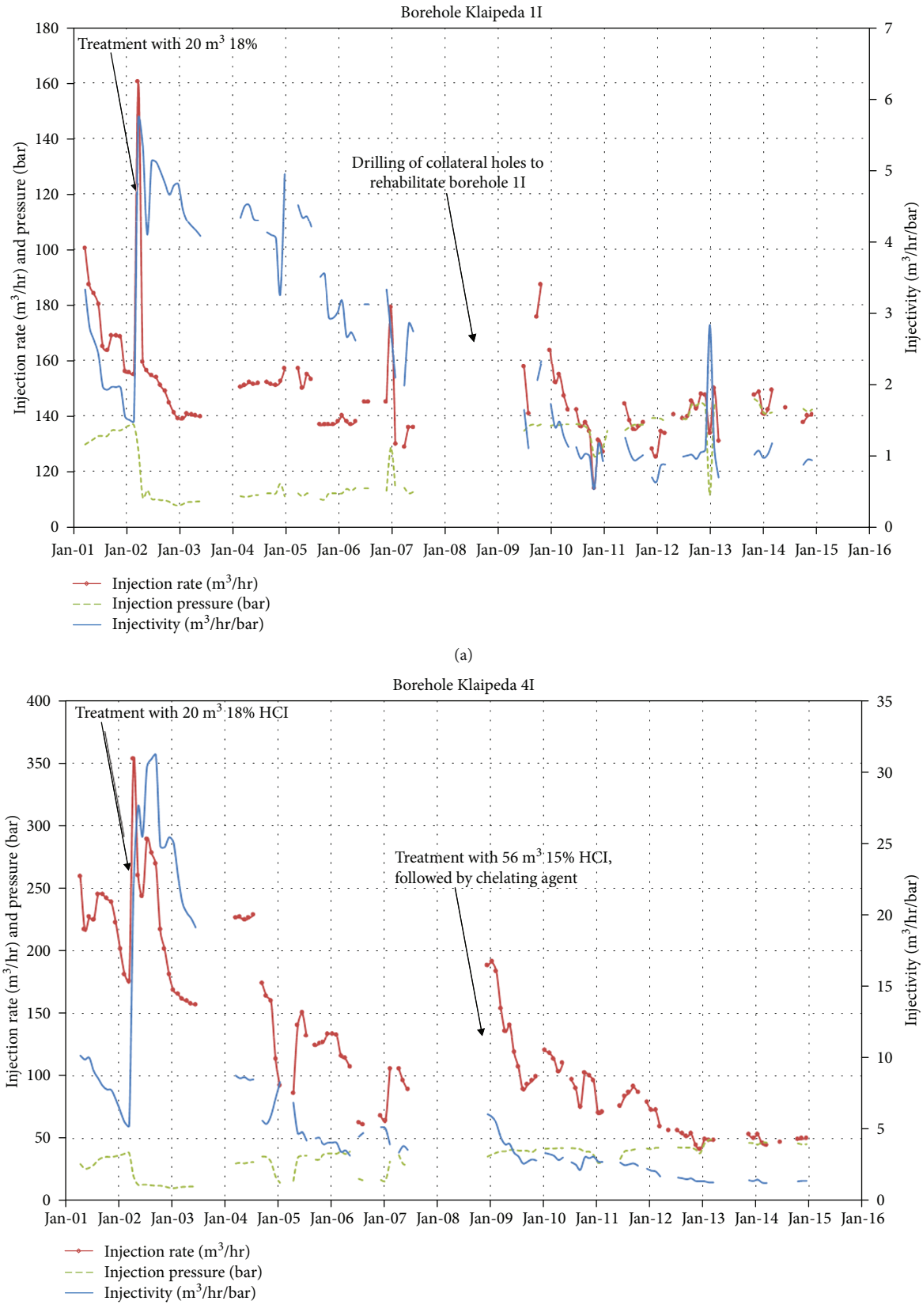

Figure 3: The decline in injectivity with time in boreholes 1I and 4I, showing timing of the most successful rehabilitation works (other works were attempted, with little visible benefit). A more detailed description of trialled remediation works can be found in [9, 11].

Table 3: Chemical composition of groundwater from Klaipeda Geothermal Demonstration Plant, showing analysis on a sample collected 5/10/2012 [17], three samples collected and analysed by GFZ-Potsdam in March-July 2016 from well 2P, and a sample collected on 5/4/17, from bulk water storage, and analysed by Glasgow University/SUERC. The final column shows standard sea water as reported by [18, 19]. An analysis of water from 2P in 2010 [9] reported concentrations of 3.2 μg/L As and 0.06 μg/L U. Additional analyses are available in GTN reports [16].

Sample date		Gerber et al. 5/10/12	2P wellhead 31/3/16	2P filter 1/4/16	2P 19/7/2016	Glasgow 2P stored water 5/4/17	Seawater
Field parameters							
pH			6.55	6.39	6.11		
EC	μS/cm		125,300	123,300	112,300		
Temperature	°C	36.4	36.4	37.2	33.6		
ORP	mV	-110	-133	-106	-88		
Dissolved O_2	mg/L		0.85	0.90	0.45		
Laboratory analysis							
Total dissolved solids	mg/L	88,523					34,483
Total organic carbon	mg/L	12					
Major cations							
Na^{2+}	mg/L	23,400	24,299	24,349	24,700	27,755	10,556
K^+	mg/L	557	616	617	656	820	380
Ca^{2+}	mg/L	6366	7558	7522	7635	7990	400
Mg^{2+}	mg/L	2175	2375	2364	2399	2450	1262
NH_4^+	mg/L	<10					0.05
Major anions							
HCO_3^-	mg/L	84*	85.4	79.3	97.6	48.8	140
Cl^-	mg/L	53,907	56,498	56,835	65,686	80,915	18,980
NO_3^-	mg/L (as NO_3^-)	<1.6	<0.6	<0.6			
SO_4^{2-}	mg/L	1606	1733	1778	2106	1555	2649
Minor elements							
F^-	mg/L		0.38	0.36	0.36		1.4
Br^-	mg/L	346	356	333	452	260	65
Fe^{2+}	mg/L		17	17	21		
Mn^{2+}	mg/L	0.86	1.0	1.0	1.1		
Li^+	mg/L	3.3	3.4	3.2	3.6		0.17
B^{3+}	mg/L	11.0	9.3	8.7	10		4.6
Si^{4+}	mg/L	6.6	4.7	4.4	4.9		4
Sr^{2+}	mg/L	143	165	166	169		13
Ba^{2+}	mg/L	0.16	0.19	0.18	0.19		0.05
Cl/Br mass ratio		156	159	171	145	311	292
Li/Cl mass ratio		6.14*E*-05	6.02*E*-05	5.63*E*-05	5.48*E*-05		8.96*E*-06
Mg/Sr mass ratio		15	14	14	14		97
B/Cl mass ratio		0.00020	0.00016	0.00015	0.00015		0.00024
$\delta^{18}O$	‰ SMOW	-4.46				-4.5	
δ^2H	‰ SMOW	-34.7				-26	
^{14}C	pmc	<0.5					
^{39}Ar	% modern	<14					
$\delta^{34}SO_4$	‰					+18.9	

*Based on a cited total inorganic carbon (TIC) of 16.6 mg/L [17]. As some of the TIC may be carbonic acid, the figure of 84 mg/L may be somewhat overestimated.

and screen (200 μm), in addition to particles of mineral precipitate. The particle size in the water is typically 4-40 μm, approximately the same size as the porosity distribution in the reservoir (see above [11]). Micron-scale filter bags and cartridges are installed immediately prior to the heat pump and

Table 4: Analyses reported in Table 3, converted to milliequivalents per litre (meq/L) and molar ratios.

Sample date		Gerber et al. 5/10/12	2P wellhead 31/3/16	2P filter 1/4/16	2P 19/7/2016	Glasgow 2P stored water 5/4/17	Seawater
Major cations							
Na^{2+}	meq/L	1018	1057	1059	1074	1207	459
K^{+}	meq/L	14.2	15.8	15.8	16.8	21.0	9.7
Ca^{2+}	meq/L	318	377	375	381	399	20
Mg^{2+}	meq/L	179	195	195	197	202	104
Major anions							
HCO_3^{-}	meq/L	1.38	1.40	1.30	1.60	0.80	2.29
Cl^{-}	meq/L	1521	1594	1603	1853	2282	535
SO_4^{2-}	meq/L	33.4	36.1	37.0	43.9	32.4	55.2
Minor elements							
F^{-}	meq/L		0.02	0.02	0.02		
Br^{-}	meq/L	4.33	4.45	4.16	5.66	3.25	0.81
Li^{+}	meq/L	0.48	0.49	0.46	0.52		0.0
Sr^{2+}	meq/L	3.26	3.77	3.79	3.86		0.30
Na/Cl molar ratio		0.67	0.66	0.66	0.58	0.53	0.86
Mg/Ca molar ratio		0.56	0.52	0.52	0.52	0.51	5.20
SO4/Cl eq ratio		0.022	0.023	0.023	0.024	0.014	0.103
Ca/Cl eq ratio		0.21	0.24	0.23	0.21	0.17	0.04
Mg/Cl eq ratio		0.12	0.12	0.12	0.11	0.09	0.19
Sr/Mg molar ratio		0.018	0.019	0.019	0.020		0.003
Sr/Ca molar ratio		0.010	0.010	0.010	0.010		0.015
Sum cations	meq/L	1532	1650	1649	1674	1836	593
Sum anions	meq/L	1560	1636	1646	1904	2331	594
IBE	%	-1%	0%	0%	-6%	-12%	0%

IBE = ion balance error.

immediately prior to the injection boreholes in order to retain particulate matter.

(iii) Corrosion. The wells contain large quantities of steel that is known to be corroding (possibly enhanced by microbial activity). As well as releasing dissolved iron to the water (see above), flakes of corroded metal are entrained in the water.

(iv) Microbial Activity/Biofouling. Both sulphate-reducing bacteria and archaea have been detected in the KGDP. There is some suggestion that activity is higher in the injection borehole environment than the abstraction wells. It has been suggested that the sodium phosphonate scaling suppressant may act as a bacterial nutrient (source of organic carbon and phosphate).

Gas bubble formation and reservoir geometry are believed to be unlikely causes of declining injectivity.

3. Groundwater Chemistry

The groundwater chemistry from the KGDP has been sampled and analysed on numerous occasions prior to and during the course of the EU DESTRESS project [9, 11, 16]. Tables 3 and 4 show a representative analysis from 2016, performed by GFZ-Potsdam, compared with published analyses from 2010 [9] and from 2012 [17] and a more recent analysis performed at the University of Glasgow and also compared with standard seawater [18, 19]. Tables 3 and 4 show that the Klaipeda geothermal water is a hypersaline brine with a total dissolved solid (TDS) content of around 90 g/L, compared with 34 g/L in seawater. The chloride content of the brine is around 60 g/L (20 g/L in seawater), while sodium accounts for two-thirds of the cation charge balance (meq/L), with calcium and magnesium accounting for one-third. The produced water has a slightly subneutral pH and is reducing in nature (oxidation reduction potential < -150 mV using a Ag/AgCl electrode) and free of dissolved oxygen. The water typically contains 1.6 to 2.4 mg/L dissolved organic carbon.

Several analyses have been carried out of the dissolved gas content:

(i) Zinevicius et al. [10] state that the brine contained 160 mL (assumed STP) of dissolved gas per litre water, of which c. 94% was N_2

(ii) Brehme et al. [11] report a gas content (believed to be degassed from the brine at c. 39°C) of 4.5%

(45 mL/L, analysis by GTN), comprising 80.1% N_2, 19.8% CO_2, 0.024% CH_4, and 0.0005% H_2S (analyses by GFZ)

(iii) Wolfgramm et al. [9] also record a gas content (degassed from the 2P brine in 2010, at c. 39°C) of 4.5% (45 mL/L), comprising 92% N_2 and 7.7% CO_2. When corrected for the content of CO_2 that remains dissolved in the water (not degassing), the dissolved gas content is corrected to 115 Ncm^3/L, of which 32.1% is N_2 and 67.7% is CO_2

Zinevicius et al.'s result [10] implies a nitrogen content of $0.94 \times 1\,\text{atm.} \times 0.16\,\text{L}/(0.0821\,\text{L atm.K}^{-1}\,\text{mol}^{-1} \times 298\,\text{K}) = 6.1\,\text{mmol/L}$ or 172 mg/L, which is significantly in excess of the solubility of N_2 (c. 24 mg L^{-1}) at 11°C and 1 atm. At the production wellhead pressure (14 bar) and the injection wellhead pressure (up to 40 bar), one would not expect the solubility to be exceeded, resulting in bubble formation, a conclusion supported by GTN [9].

On the basis of isotopic evidence, the brines of the Baltic basin have been interpreted [17] as a mixture between three hypothetical end members:

(1) A relatively modern (interglacial or more recent) meteoric water, with $\delta^{18}O$ = c. -10.4‰ (see Figure 4)

(2) A glacial meltwater component, with a depleted $\delta^{18}O$ < c. -18‰, a poorly evolved hydrochemistry and elevated noble gas concentration

(3) An ancient hypersaline brine (Cl^- in excess of 90 g/L), with an enriched $\delta^{18}O$ > c. -4.5‰ and rather low noble gas concentrations. The brine is hypothesised to originate from evapoconcentration of seawater, followed by water-rock interaction

For components (1) and (2), ^{81}Kr data indicated ages ranging from 300,000 years to 1.3 Ma. For the deep brine component, radiogenic noble gas concentrations ($^4He^*$ and $^{40}Ar^*$) suggest an age in excess of 1 Ma and tentatively in the range of 3 to 5 Ma. In the case of the Klaipeda boreholes, proportions (based on water) have been suggested [17] of

(i) 38 ± 8% meteoric water (component 1)

(ii) 2 ± 4% glacial meltwater (component 2)

(iii) 60 ± 5% hypersaline brine (component 3)

Various features of the analyses in Tables 2 and 3 support Gerber et al.'s interpretation [17]. The brine is enriched in calcium relative to evapoconcentrated seawater, which must be due to water-rock interaction (the Ca^{++}/Cl^- meq ratio is typically just over 0.2 in the brine but only 0.04 in seawater). Similarly, the Mg^{++}/Cl^- ratio exceeds seawater—unsurprising, given the extensive presence of dolomite in the Upper Devonian sequence (Figure 2). The ratio of sulphate to chloride is less in the brine (just over 0.02 as meq) than in seawater (0.103), suggesting that gypsum has been removed from the brine, by precipitation either during evaporative upconcentration or during residence in the aquifer as calcium enters solution from water-rock interaction. The sulphur isotope signature of the sulphate in the brine (+18.9‰) is slightly lower than modern seawater (+21‰), which is consistent with Gerber et al.'s hypothesis of an evapoconcentrated brine admixed with fresher meteoric of glacial meltwater recharge. However, the drilling logs note the presence of evaporite minerals, including gypsum (in the Kemeri sandstones) and dolomite (in the overlying Upper Devonian) in the Devonian sequence. The slightly depressed sulphate isotopic signature could also be due to equilibration and sulphur exchange with Devonian evaporite gypsum (which is believed to have potentially had a depleted ^{34}S content relative to modern seawater [24]).

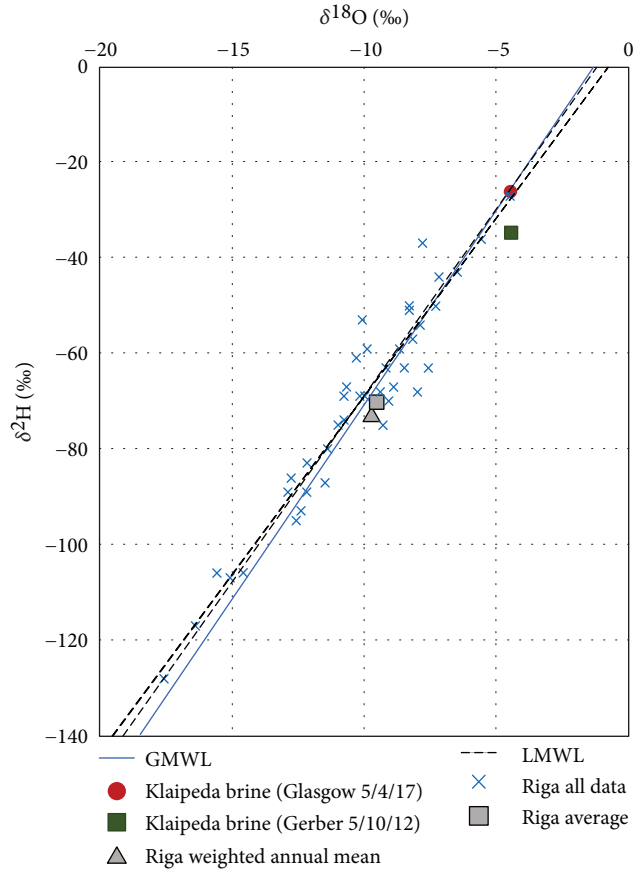

FIGURE 4: Stable ^{18}O and ^2H data for the water sample documented from October 2012 [17] and the water sample of 5/4/17 analysed in Glasgow, compared with available monthly data for isotopic composition of precipitation from the WMO Riga meteorological station (station no. 2642200, 1980-89). The dashed lines show possible interpretations of the local meteoric water line (LMWL) and global meteoric water line (GMWL). Data from [20]. Note that Quaternary intertill aquifers in eastern Lithuania typically contain groundwater with a $\delta^{18}O$ of -10.0 to -11.2% (i.e., similar to meteoric water [21]). Lithuanian Devonian aquifers [22] of <500 m depth typically contain groundwater with $\delta^{18}O$ of -10.2 to -13.0%; below 500 m depth, the signatures become less negative (as high as -4.5% in borehole Naumiestis 1). See also [23].

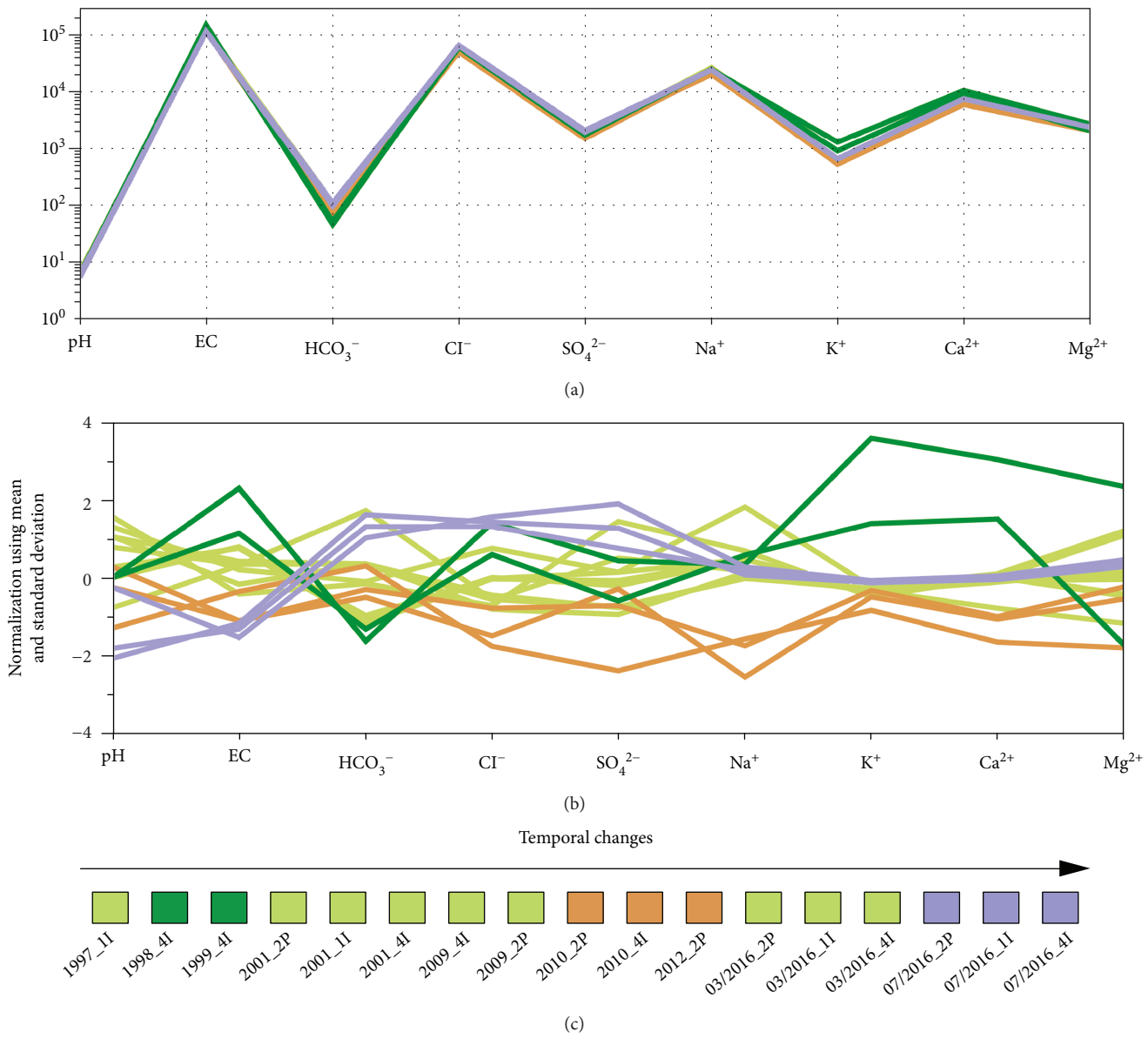

Figure 5: Absolute concentrations (a) and normalised concentrations (using mean and standard deviations) (b) of major constituents in the Klaipeda brines plotted in Schöller diagrams. Temporal changes in water composition and the colour-coded groups of samples (identified using self-organizing maps) are shown in the lowermost plot (c).

The Cl/Br ratio is significantly lower (typically 150 to 170) than that in seawater (c. 290). Given that atmospheric precipitation typically has a ratio of 50-100 and shallow groundwater 100-200 [25], this is consistent with the mixing model described above [17]. The low ratio could also conceivably be partially explained by precipitation of halite during evapoconcentration of the brine, if salinity reached high enough levels for this to occur. The B/Cl mass ratio in the brine (0.00015 to 0.0002) is slightly lower than seawater (0.00024). The Mg/Sr mass ratio is 14-15, much lower than seawater (97, according to [18] or 168 according to [26]). The observed value is a characteristic of highly saline groundwater in modern environments (e.g., Afghanistan [27]).

4. Temporal Changes in Klaipeda Groundwater Chemistry

The fluid composition from the Klaipeda wells has been observed via sampling at irregular intervals during the period 1997 to 2017. The groundwater quality is rather stable, with the main ionic components of the water being Cl^-, Na^+, Ca^{2+}, Mg^{2+}, SO_4^{2-}, and HCO_3^-. The composition of the fluid does appear, however, to have exhibited some modest variation over time, which may be related to the dynamic nature of the reservoir development (but could also reflect the fact that the analyses of a high concentrated brine, involving laboratory dilutions prior to analysis, have been carried out at different laboratories according to different protocols).

Fluid compositions have been analysed by neural network clustering, using self-organizing maps (SOM), which can be used for the clustering and classification of multidimensional data [28]. Clustering separates the samples into four groups (Figure 5). The largest group of samples is visualised in light green; the dark green samples occurred in 1998/1999 in well 4I. The orange group denotes samples from 2010/2012, and blue samples relate to the most recent sampling campaign. The normalized Schöller diagram shows (admittedly rather minor) differences between the different groups and some individual samples in specific element concentrations.

The light green samples typically represent the most "typical" ionic concentrations, which is also the initial water composition in well 1I. The dark green type is the starting composition in well 4I before it evolves into the "typical" Klaipeda water composition. Samples from 2010/2012 (orange) generally have the lowest element concentrations. The temporal trend of the four groups indicates a decrease in electrical conductivity (EC) and an increase of HCO_3^- between 1997 and 2016. K^+, Ca^{2+}, and SO_4^{2-} initially decrease until reaching their lowest values in 2010/2012, before increasing again. The recent water type shows increased SO_4^{2-}, Cl^-, and HCO_3^{2-} concentrations.

The slight tendency to decreasing salinity (EC) could suggest that continued abstraction of brine is inducing leakage of less saline groundwater from higher stratigraphic levels. This ingress of less saline water may possibly lead to enhanced dissolution of carbonate minerals and slightly increasing alkalinity.

5. Potential for Mineral Precipitation and Clogging

5.1. Hydrogeochemical Modelling. Previous work [17] has noted that the Klaipeda brines were likely to be approximately saturated with respect to calcite, gypsum, dolomite, and celestite ($SrSO_4$). Modelling of the Klaipeda brine of 1/4/16 (due to its extremely good ion balance and to the fact that it is intermediate in salinity between the 2012 sample [17] and the 2017 Glasgow sample) has been undertaken with PHREEQC Interactive version 3.3.5 [29], using the Pitzer database, which is appropriate for highly saline waters [30, 31]. The results are shown in Table 5, firstly calculated at 37°C (the abstracted water temperature) and secondly calculated at 11°C, approximately representative of reinjection temperature, following heat extraction by the absorption heat pumps.

The modelling suggests that the water would be in equilibrium with a CO_2 partial pressure of $10^{-1.6}$ atm. It confirms that the brine remains significantly undersaturated with respect to the evaporite minerals epsomite, thenardite, sylvite, halite, magnesite, and mirabilite. The water is approximately saturated with respect to barite, gypsum, quartz, and celestite (Figure 6). The modelling suggests that the water is very slightly oversaturated with respect to calcite and dolomite, although this index is highly dependent on the reliability of the pH determination, and one can hypothesise that the sampling of a deep CO_2-containing groundwater might allow

Table 5: Calculated saturation indices for the Klaipeda 2P brine sampled on 1/4/16, at 37°C and 11°C, using PHREEQC Interactive version 3.3.5 [29] and the Pitzer thermodynamic database.

Phase	SI (37°C)	SI (11°C)	Formula
Dolomite	0.58	0.04	$CaMg(CO_3)_2$
Calcite	0.35	0.11	$CaCO_3$
Celestite	0.13	0.04	$SrSO_4$
Aragonite	0.04	-0.1	$CaCO_3$
Gypsum	0.01	0.06	$CaSO_4{\cdot}2H_2O$
Barite	-0.08	0.27	$BaSO_4$
Anhydrite	-0.15	-0.43	$CaSO_4$
Quartz	-0.18	0.22	SiO_2
Chalcedony	-0.57	-0.25	SiO_2
Magnesite	-0.63	-0.68	$MgCO_3$
Goergeyite	-1.25	0.5	$K_2Ca_5(SO_4)6H_2O$
SiO_2 (amorphous)	-1.42	-1.18	SiO_2
Halite	-1.71	-1.67	NaCl
Mirabilite	-2.92	-1.78	$Na_2SO_4{\cdot}10H_2O$
Sylvite	-3.05	-2.77	KCl
Thenardite	-3.1	-3.23	Na_2SO_4
Epsomite	-3.19	-2.91	$MgSO_4{\cdot}7H_2O$
Brucite	-5.25	-6.26	$Mg(OH)_2$

degassing of CO_2 at the wellhead and a concomitant pH rise. It is perhaps more instructive to note those minerals whose saturation index increases to more supersaturated values on cooling and which are at risk of precipitating within heat exchangers, pipework, and reinjection wells: prominent amongst these are quartz (although precipitation might be expected to be kinetically constrained) and the sulphate minerals, barite, and gypsum. Due to the massive superiority of calcium in the water's chemical composition, gypsum must be regarded as the prime suspect for chemical "scaling" on cooling.

Although redox-sensitive species are not explicitly modelled in Table 4, the presence of mg/L quantities of dissolved iron and manganese in a moderately reducing water (ORP below -100 mV) implies that these elements are present in their reducing (Fe^{2+} and Mn^{2+}) states. The event of any contact between these dissolved reduced metals and atmospheric oxygen in the abstraction-heat exchange-reinjection process risks the precipitation of manganese oxides (MnO_2) or ferric oxyhydroxides ($Fe(OH)_3$) and the parallel risk of biofilm formation by iron bacteria. Indeed, the fact the small quantities of oxygen have been repeatedly detected by GFZ analyses of brine within the plant of KGDP suggests that it is difficult to wholly exclude oxygen.

5.2. Potential for Gypsum Precipitation and Clogging. We have seen, above, that the two sulphate minerals, whose saturation indices increase with declining temperature and which become oversaturated on cooling, are gypsum and barite (Table 5). Indeed, prior to the implementation of phosphonate inhibitor in Dec. 2003, gypsum was identified in the sumps of the injection wells [16]. PHREEQCI was further

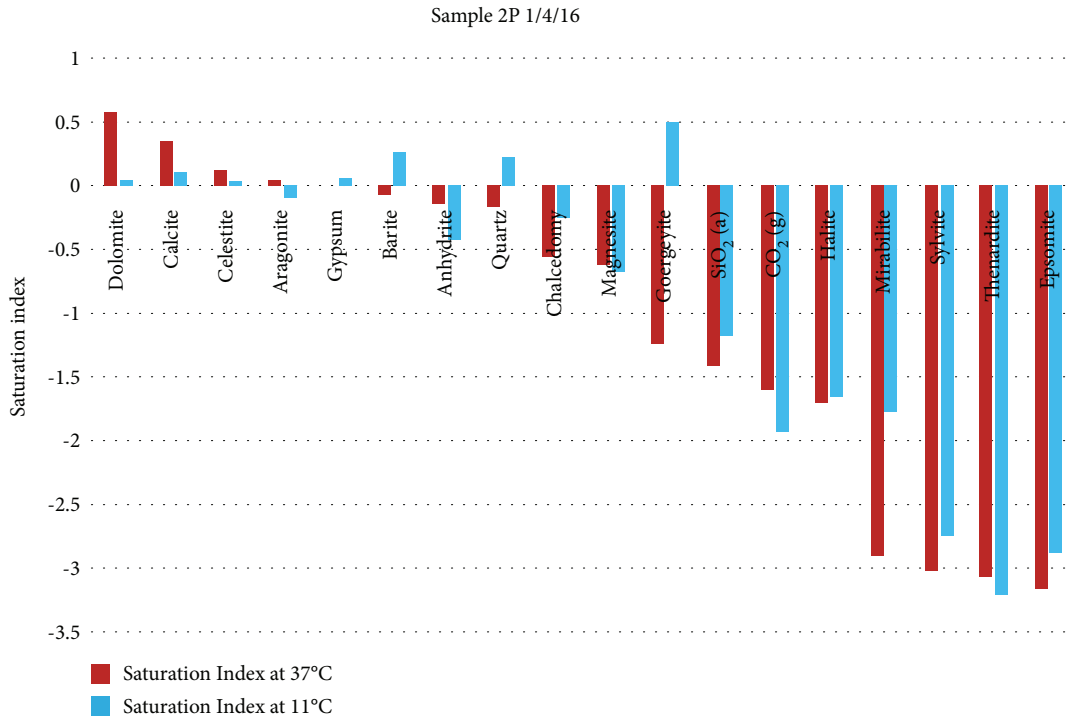

Figure 6: Diagram illustrating the relative saturation indices of various minerals at 37°C and 11°C for the Klaipeda 2P water sample of 1st April 2016 (from Table 4).

used to calculate the amount of gypsum and barite that would precipitate from solution if the brine is cooled to 11°C (nominal reinjection temperature), with the minerals in question achieving a saturation index of 0 (Table 6). We can thus see, from Table 6, that

(i) the precipitation potential of barite is negligible compared with gypsum

(ii) every kg of water has the potential to precipitate 378.8 mg gypsum on cooling to 11°C

(iii) given that the water's density is c. 1.09 kg/L, each litre of water has the potential to precipitate 412.9 mg gypsum on cooling to 11°C

Table 6: Calculated potential loss of gypsum and barite per kg brine, on cooling to 11°C (brine from well 2P 1/4/17).

	Before (37°C) mol/kg H_2O	After (11°C) mol/kg H_2O	Loss mol/kg H_2O
Ca	1.884*E*-01	1.862*E*-01	2.200*E*-03
Ba	1.316*E*-06	7.933*E*-07	5.227*E*-07
$SO_4^=$	1.858*E*-02	1.637*E*-02	2.210*E*-03
Gypsum			2.200*E*-03
Barite			5.227*E*-07
			mg/kg H_2O
Gypsum			378.8
Barite			0.12

5.3. Phosphonate Dosing. The significant potential for gypsum clogging at the KGDP can be illustrated by the fact that, during the early years of operation, pipework at the plant rapidly became almost completely blocked by solid cylindrical plugs of crystalline gypsum (requiring full rehabilitation in 2003-2004). In response to this, since Dec. 2003, the abstracted brine has been dosed with the scale inhibitor Labuxan 206, which appears to have successfully suppressed the formation of gypsum in the surface plant at KGDP. Labuxan 206 is c. 50% solution of the sodium salt of diethylene triamine pentamethylene phosphonic acid (DTPMP or $C_9H_{26}N_3P_5O_{15}$) in water. In other words, it is a sodium phosphonate (Figure 7), with 10 possible proton dissociation sites (all of whose dissociation constants are quantified [32, 33]).

Thus, the molecule can, as conditions become more alkaline, form an anion with up to 10 negative charges [32] and is thus rather effective at binding cations (especially calcium) into a complex soluble structure. The fact that calcium is removed from solution into a complex phosphonate ion means that the saturation indices of gypsum, calcite, etc. decrease and precipitation of those minerals is suppressed. Phosphonates are thus widely used in medicine and industry (especially in the hydrocarbon and electrical industries, particularly in deep wells and cooling towers) for corrosion- and scale-control and as chelants and dispersants, due to their ability to complex with and mobilise a wide variety of otherwise potentially poorly soluble cations. They are regarded generally as "practically nontoxic" and applied at rates of a few mg/L [32]. Their environmental behaviour and potential for degradation have been reviewed by [34].

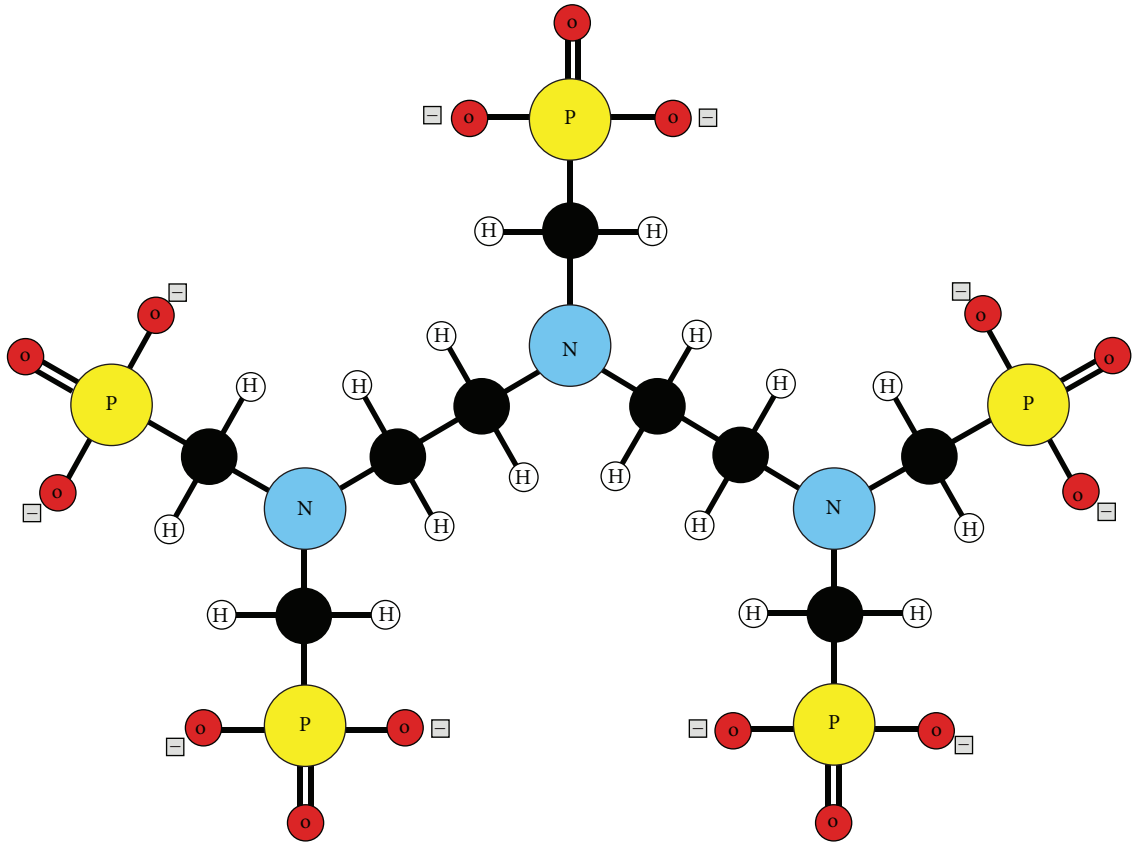

Figure 7: Schematic structure of DTPMP fully deprotonated anion, with 10 negative charges—black circles represent carbon atoms [33].

Table 7: Results of phosphonate monitoring (2010), after [9].

Measuring point (Figure 8)	T2	T2a	T12
Location	Production well 2P, prior to phosphonate dosing	Production well 2P, immediately after phosphonate dosing	Injection well 4I, prior to injection
Date	16/7/10	16/7/10	16/7/10
Total phosphate, expressed as PO_4^{3-}	0.132 mg/L	3.89 mg/L	1.56 mg/L
Orthophosphate as PO_4^{3-}		0.14 mg/L	

In 2010, the daily consumption was 15 L of 50% DTPMP solution at well 2P [9]. In 2010, GTN monitored phosphonate concentrations at three points in the Klaipeda geothermal system [9].

The data in Table 7 imply that the brine contains around 0.13 to 0.14 mg/L phosphate, which is increased to 3.89 mg/L by phosphonate dosing. Thus, the dosing rate of phosphonate is around 3.76 mg/L as PO_4^{3-}. Around 38% is still present as phosphonate by injection. Bottle tests [9] indicated that the actual dosage rate of DTPMP is close to the optimum. A higher dosage produced iron-rich residues and colourless phosphonate residue. Testing and monitoring indicated that DTPMP dosing does not completely prevent the occurrence of gypsum crystals, as these have been identified during bottle tests and during monitoring at various points on the production-reinjection line, including after the 1 μm filters at the injection wells (sample point T8a in Figure 8) [9].

The use of DTPMP is specifically used [35, 36] to suppress calcium scale formation in deep oil and gas wells by so-called "squeeze" treatment. An acidic solution (or "pill") of DTPMP is initially injected into the formation. It is supposed that this reacts with calcium (dissolved from the formation by the acid) to produce a calcium phosphonate precipitate. As the oil/gas well starts producing, the pumped formation fluid initially contains a relatively high concentration of phosphonate (return of surplus dissolved inhibitor), then contains a concentration of a few mg/L (potentially in equilibrium with an amorphous or microcrystalline calcium phosphonate precipitate). As production flow of formation water continues, any calcium phosphonate precipitate is supposed to "harden" to a crystalline phase, in equilibrium with a return concentration of typically <1 mg/L phosphonate. The residual phosphonate concentration from the slow dissolution of the calcium phosphonate precipitate inhibits scale formation in the well. Indeed, the crystallisation of the

calcium phosphonate precipitate is reported [35] to be a two-stage process, with the initial precipitation of an amorphous, relatively soluble calcium phosphonate phase. On contact with flowing production water, this hardens to a well-crystallised phase, at least 2 orders of magnitude less soluble. It is suggested [36] that the crystallisation may even be a three-stage process. It is assumed that the precipitate is represented by the formula Ca_3H_4DTPMP, although the calcium mole fraction may increase [36] from 2.5 to up to 4.5 as production flushing and progressive crystallisation increases. In other words, in deep oil and gas wells, the prior injection of DTPMP to the formation is deliberately intended to create a solid-phase reservoir of phosphonate precipitate in the formation, which is slowly released to the production well for purposes of scale formation. This leads us to query, could the introduction of DTPMP prior to injection at Klaipeda also lead to precipitation of a Ca-DTPMP precipitate in the formation, which is not recovered but which accumulates over time?

It is suggested [35] that the solubility product (K_{sp}) of the calcium phosphonate precipitate can be given by $K_{sp} = (Ca^{2+})^3\{H^+\}^4(Phn^{10-})$ and is typically around 10^{-50} to 10^{-55} and that it is dependent on ionic strength (I) and temperature (T): e.g., for the crystalline phase:

$$pK_{sp\,crystalline} = \frac{58.95 - 2084.5}{T + 0.048I^{0.5}}. \quad (1)$$

Thus, for the Klaipeda brine at 11°C (284 K), with an ionic strength of 1.96 (from PHREEQC modelling), p$K_{sp\,crystalline}$ = 51.7. The solubility decreases as temperature increases, implying, at Klaipeda, that the reequilibration of a cool injected fluid with a warm ambient reservoir temperature would enhance precipitation potential. In the Klaipeda brine,

(i) the molality of calcium is 0.188 mol/kg

(ii) the pH is c. 6.1 to 6.4

(iii) the added concentration of phosphonate is around 3.76 mg/L as phosphate = 0.0396 mM (as phosphate). As each molecule of DTPMP contains 5 phosphate units, the concentration of phosphonate is thus 0.0079 mM or 7.9 μM

A case study from no. 4 oil well, Odem, Texas, is documented [35], where

(i) the concentration of calcium is 0.011 M

(ii) the pH is 6.37

(iii) the "plateau" concentration of phosphonate is 0.86 μM

A further case study [35] from an anonymous "Well A," North Sea, had the following characteristics:

(i) The concentration of calcium is 0.006 M

(ii) The pH is 6.60

(iii) The "plateau" concentration of phosphonate is 3.7 μM

In both the North Sea and Texas cases (temperatures of 71-110°C), it appeared that the produced fluid was in equilibrium with a solid calcium phosphonate phase in the formation. The phosphonate and calcium concentrations in the Klaipeda system are higher than both these cases, although the reservoir temperature is lower. Nevertheless, there remains a strong possibility that calcium phosphonate could be precipitating within the reservoir. The potential precipitation of calcium phosphonate from the Klaipeda waters is unlikely to exceed c. 4 mg/L, which is modest compared with overall precipitation potential of gypsum at c. 400 mg/L. It should be noted, however, that laboratory experiments have visually observed the formation of a fibrous phosphonate precipitate in pore throats in an artificial porous medium [37].

5.4. Gypsum as a Contributor to Injectivity Decline? It is already known that there is a potential precipitation risk from gypsum. The dosing of the reinjected brine with DTPMP was undertaken initially to suppress gypsum clogging in pipework, at which it was largely successful. However, monitoring [9] has shown that precipitation of microparticles of gypsum in the system continues to occur, even after dosing. We have also seen, above, that there may be potential for Ca-DTPMP to form a solid precipitate in the formation. If this occurs, then the suppression effect of the DTPMP may be partially lost, and gypsum precipitation could still have the potential to occur within the reservoir. If we assume that the phosphonate, while effective at short-term suppression of massive gypsum precipitation in pipework, is not necessarily effective at suppressing longer-term gypsum precipitation in the reservoir, then each kg of cooled brine could have the potential to precipitate up to 0.38 g gypsum.

If we further assume that the injection rate of each injection borehole at Klaipeda has been on average c. 50 m^3/hr (13.9 L/s = 1,308,000 kg/day, Figure 3), that the aquifer has a porosity of 26%, and that the injection boreholes have been operating for 15 years for around 50% annual running time (2740 days), then the total quantity of injected water is around 3.3×10^6 m^3 (3.6×10^9 kg), sufficient to fill a volume of 12.6×10^6 m^3 aquifer. Assuming the effective aquifer thickness is 70 m, this volume represents a cylinder of radius 240 m. We have already estimated a gypsum precipitation potential of 1.36×10^6 kg of gypsum (5.85×10^2 m^3, assuming a gypsum density of 2.32 g/cm^3). If gypsum precipitation was evenly distributed throughout this aquifer volume, it would result in only 0.018% occlusion of pore space.

If we assume a bulk aquifer volumetric heat capacity of 2.2 MJ/m^3/K (water = c. 4.19 MJ/m^3/K), then the volume of cooled aquifer is estimated as 12.6×10^6 $m^3 \times 0.26 \times 4.19$ MJ/m^3/K/2.2 MJ/m^3/K = 6.26×10^6 m^3, equivalent to a cylinder of radius 169 m (and probably less, given thermal leakage into overlying and underlying strata). If gypsum precipitation occurs evenly throughout the cooled volume, it now occludes an estimated 0.036% of the pore space.

Both the above calculations assume an evenly distributed precipitation of gypsum in the aquifer volume. This is, of course, highly unlikely, as gypsum precipitation is kinetically rapid and most likely to occur when the injected water is at its coolest—i.e., in the vicinity of the injection well. Figure 9 shows the proportion of pore space filled with gypsum, assuming that precipitation occurs exclusively within a given radius of the injection well. The figure indicates that if gypsum is precipitated within 30 m of the injection borehole, then porosity occlusion is significant (>1%). If it occurs within 10 m of the borehole, it becomes very significant (>10%).

6. Empirical Observation—Mineral Precipitation and Particulates Observed in Filters

The potential saturation and precipitation of minerals suggested by the hydrogeochemical modelling have been confirmed and complemented by empirical observation of

(i) filter residue captured near the production and injection wellheads from bag and cartridge (1 μm mesh) filters installed on the fluid circulation system (Table 8, Figure 8)

(ii) water samples, taken from various points in the plant and subject to fine manual filtration (July 2010–Table 9). Here, cellulose acetate filters with aperture 0.45 μm (and in one case of 3 μm) were applied. After filtration, the filters were flushed with distilled water in order to reduce secondary evaporative formation of halite and gypsum from any residual liquid brine. The samples were dried at room temperature. They were examined under binocular microscope and also by scanning electron microscope (SEM), the SEM samples having been coated with carbon

(iii) a bailer sample from well 1I, taken in 2014 (Table 10)

In filter bag samples from 2010, relatively large gypsum crystals were a significant component of the filter bag residue, while iron sulphide crystals were also observed. Although the filter bag is located after the inhibitor introduction point, it is likely that the gypsum had been formed in the production well and had not been redissolved by the inhibitor. The filter bag residue from 2016 contained a far greater proportion of reservoir grains and corrosion fragments. In general, the residue from bag and cartridge filters from 2016 was less rich in gypsum and richer in typically comprised three main components: corrosion particles, reservoir grains, and precipitated minerals. The residue contains grey to brown-reddish particles in the mm (up to 1 cm) size range. The detrital grains from the reservoir include quartz, biotite, calcite, dolomite, and microcline. The chemically precipitated materials included gypsum, anhydrite, and halite (although this is presumed to have formed by evaporative drying on the surface of the sample after sampling). Corrosion particles consist of lepidocrocite, magnesioferrite (which is documented as a steel corrosion product in saline conditions [38]), and iron sulphide.

In the manually filtered samples from July 2010, the solids highest loads were found at the production well at a point prior to the injection of phosphonate. The particulate loads at the production well consist mainly of copper-iron sulphides, detrital particles from the reservoir, and gypsum crystals [9]. Following the bag filter between the phosphonate dosing point and the heat exchanger, the solids loads decrease significantly and comprise mainly iron-copper-(zinc) sulphide scales. The lowest solids loadings were found after the heat exchanger. Here, they were dominated by iron sulphides/oxyhydroxides, although contents of metals such as titanium, chromium, and nickel in the sulphide scales had increased significantly, suggesting corrosion in the heat exchanger. Calcium carbonates and clay minerals were also identified after the heat exchanger, as were small quantities of phosphorus compounds (suggesting some reprecipitation of phosphonate inhibitor). Filtration through filter cartridges prior to injection at 4I does not appear to result in a further decrease in suspended solids. On the injection side of the system, the gypsum content of the samples was relatively low, testifying to the success of the inhibitor and bag filters; gypsum was, however, sporadically detected, even after the 1 μm cartridge filters, in very small quantities.

The bailer sample from the 1I sidetrack (2014) was a compact, sticky mass of grey to beige material, with a soapy texture. It showed similar minerals to those documented and in Table 2 representing sandstone, claystone, and corrosion material (but also including the presence of cuprite and jacobsite).

7. Discussion and Conclusion

The hypersaline brine (salinity c. 90 g/L) from the Devonian sandstone/siltstone reservoir at the Klaipeda Geothermal Demonstration Plant (KGDP) is dominated by sodium and chloride in its ionic chemistry. Around two-thirds of the cation content (as meq/L) is accounted for by sodium; the bulk of the remainder is calcium and magnesium. The hydrogen and oxygen stable isotope composition is relatively undepleted in ^{2}H and ^{18}O ($\delta^{18}O$ = c. -4.5‰), while the $\delta^{34}S$ is relatively "heavy" at +18.9‰. The hydrochemical data, solute ratios, and stable isotope composition all support the previous hypothesis [17] that the groundwater is dominated by a hypersaline brine derived from evapoconcentrated seawater, modified by water-rock interaction and admixed with smaller quantities of more recent glacial meltwater and/or interglacial recharge. The chemistry of the Klaipeda water has remained relatively unchanged during the period of operation of the KGDP, although statistical analysis tentatively points towards a slight declining trend in salinity and increase in bicarbonate. One can speculate that this may be due to abstraction inducing a small component of leakage of fresher water from overlying strata, in turn leading to an increase in potential for carbonate dissolution.

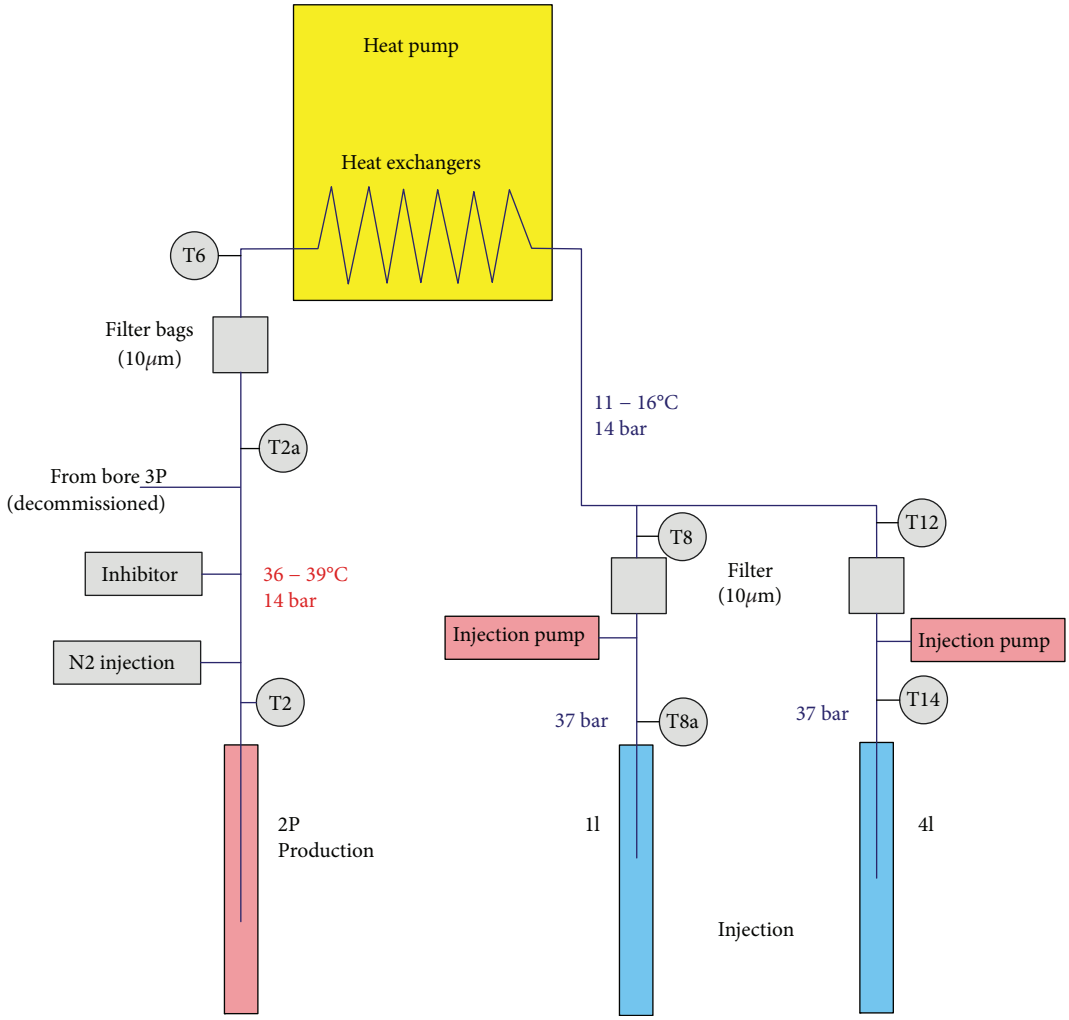

Figure 8: Schematic of KGDP, showing locations of sampling (T2, T2a, etc.).

Table 8: Minerals identified (by X-ray diffraction) in filter residue from bag and cartridge filters installed on the KGDP brine pumping-injection line. The halite is likely to represent drying by evaporation of the filter surface.

Sample date	Apr 2016	Jul 2016	Apr 2016	Jul 2016	Jul 2016
Filter sample	KLA 2P bag filter		KLA 1I bag filter		KLA 1I cartridge filter
Minerals	Magnetite	Quartz	Halite	Halite	Quartz
	Quartz	Magnetite	Lepidocrocite	Lepidocrocite	Halite
	Gypsum	Halite	Gypsum	Quartz	Lepidocrocite
	Spineloid (low)		Biotite	Magnetite	Anhydrite
	Microcline				Gypsum
	Dolomite				Calcite
	FeS				Magnesioferrite

The injectivity of the two injection boreholes 1I and 4I has declined dramatically during the operational period, severely limiting the potential output of the KGDP. Initially (up to c. 2003), the water produced from 2P and (especially) 3P was precipitating large quantities of massive crystalline gypsum in the surface pipework and (one must assume) in the reinjection boreholes. This led to a major rehabilitation program, the decommissioning of 3P and the introduction of sodium polyphosphonate dosing of the brine following abstraction. This appears to have been largely successful on

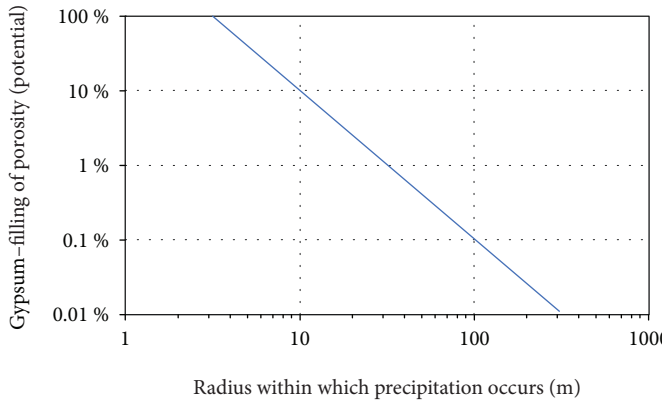

Figure 9: Percentage of pore space potentially filled by gypsum, assuming gypsum precipitation occurs entirely within a given radius of the injection well (assuming effective porosity = 26%).

Table 9: Determination of particle loads from manual filtration of Klaipeda brines at various sampling points in July 2010 [9].

Location (Figure 8)	Filter aperture (μm) μm	Quantity of water filtered Litre	Mass of filter residue mg	Loading of filtered suspended solids mg m^{-3}	Identified particulate matter, sorted by quantity
T2. Production wellhead (2P) prior to phosphonate dosing	0.45	44.25	3.4	76.8	*$CuFeS_2$, iron (Cu, Zn) sulphides, iron hydroxides/oxides*, K-feldspar, $Ca(Mg)CO_3$, clay minerals, SiO_2
T2. Production wellhead (2P) prior to phosphonate dosing	0.45	44.25	2.6	58.8	
T2a. After phosphonate dosing, prior to bag filter	0.45	44.25	2.6	58.8	*Iron (Cu, Zn) sulphides, iron hydroxides/oxides*, $CaCO_3$, SiO_2, Cu, Zn sulphides, $CaSO_4$
T2a. After phosphonate dosing, prior to bag filter	3	53.7			*Iron (Cu, Zn) sulphides*, $CaCO_3$, iron hydroxides/oxides, SiO_2, $CaSO_4$
T6. After bag filter, prior to heat pump heat exchanger	0.45	44.25	1.01	22.8	*$CuFeS_2$, iron (Cu, Zn) sulphides, K-feldspar, clay minerals*, iron hydroxides/oxides, $CaCO_3$, SiO_2, $CaSO_4$
T6. After bag filter, prior to heat pump heat exchanger	3	54			*Iron hydroxides/oxides, iron sulphides*
T8. After heat pump heat exchanger, prior to cartridge filter and injection pump at injection well 1I	0.45	45	0.7	15.6	*Iron (Ni, Zn) sulphides Fe, Cr particles, iron hydroxides/oxides, clay minerals*, $CaCO_3$, SiO_2, $CaSO_4$ +P, $Mg(Ca)CO_3$, CuZn sulphide
T8a. After cartridge filter and injection pump at injection well 1I	0.45	44.25	0.2	4.5	*Iron hydroxides/oxides, iron (Cu, Ni) sulphides*, $CaSO_4$, clay minerals, FeCr particles, zinc sulphide, SiO_2
T12. After heat pump heat exchanger, prior to cartridge filter and injection pump at injection well 4I	0.45	44.25	1	22.6	*Iron sulphides, $CaCO_3$, iron hydroxides/oxides, clay minerals (bearing K, Mg, Fe)*, SiO_2, FeCr particles
T14. After cartridge filter and injection pump at injection well 4I	0.45	45	1.4	31.1	*$CuFeS_2$, Fe, Cr particles, SiO_2, K-feldspar*, $CaCO_3$, Ca is always present, $CaSO_4$?

Italic text indicates >10% of particulates.

Table 10: Minerals identified (by X-ray diffraction) in the bailer sample from borehole 1I sidetrack in 2014.

Bailer sample	1I Bailer clast	1I Bailer fine	1I Bailer coarse	1I Bailer mag
Minerals	Quartz	Quartz	Quartz	Magnesioferrite
	Muscovite	Halite	Dolomite	Quartz
	Chlorite	Magnetite	Cuprite	Calcite
	Kaolinite	Cuprite	Jacobsite	
	Halite	Illite	Magnetite	
		Kaolinite	Chlorite	
			Biotite	

preventing gypsum precipitation in the surface plant and the reinjection boreholes but has not halted or reversed the injectivity decline.

Various attempts as rehabilitating the injection boreholes have resulted in little improvement or, at best, only temporary gains in injectivity. The most successful was the acidisation of both boreholes in 2002 with 20 m^3 18% hydrochloric acid, but even in this case, the injectivity gains were temporary.

The potential causes of declining injectivity have already been examined [11]. Microbiological and chemical injectivity occlusion mechanisms were considered, although the most likely culprits were tentatively considered to include the clogging of the formation by steel corrosion particles/residues and by fine particles in the reservoir. These latter could be detrital formation grains entrained in water from the abstraction boreholes (known to contain particulates of dimension 4-40 μm—i.e., approximately the same size as the porosity distribution in the reservoir), although these should be retained by bag and cartridge filters (1 μm mesh) on the production and reinjection pipelines. Fine (clay) particles could also be redistributed within the reservoir in the immediate vicinity of the reinjection boreholes, by injection flows themselves, and indeed, gamma logging provides some evidence for this having occurred [11]. Clogging by exsolving gas bubbles has been deemed unlikely due to the rather high injection pressures.

This paper suggests that one should not wholly exclude the significance of chemical precipitates as an injectivity clogging mechanism. Thermodynamic modelling suggests that gypsum and barite are both thermodynamically likely to precipitate on cooling, while iron and manganese oxyhydroxides could form if the water is exposed to oxygen (and indeed have been identified in filter residues, although it is unclear if these are corrosion residues or primary chemical precipitates). The gypsum precipitation potential of the reinjected water, following cooling from 37°C to c. 11°C, is calculated as 413 mg per litre. Although the sodium polyphosphonate inhibitor appears to be effective at suppressing large-scale gypsum precipitation in the surface plant, it has been demonstrated that micron-scale gypsum precipitates are still forming. Given that polyphosphates are known to form calcium polyphosphonate precipitates in hydrogeological reservoirs, it is unclear whether the inhibitor continues to suppress gypsum precipitation in the reservoir environment. If gypsum precipitation is primarily occurring within 30 m of the injection borehole, then it could account for occlusion of >1% of porosity (more than adequate to cause occlusion of pore throats); if it occurs within 10 m, the porosity occlusion could exceed 10%. Moreover, it is known that fibrous precipitation of calcium polyphosphonate itself can lead to clogging of pore throats [37].

It has been shown that 80% of the reservoir pore space has an aperture of between 3 and 40 μm [11]. If micron-scale chemical precipitates, corrosion residues, or particles or fine-grained reservoir clasts are being mobilised into the injection borehole, or within the injection reservoir environment, it is quite conceivable that they are occluding pore throats. It has been observed that the productivity of the injection boreholes 1I and 4I, when back pumped, significantly exceeds the injectivity. One mechanism for explaining this is that micron-scale particles, forced into pore throats by continued injection, would potentially occlude those pore throats. During temporary back pumping, the particles may be pulled "back" out of the pore throats into the larger pore void (say c. 10 μm), releasing the flow occlusions, very similar to a conventional one-way ball valve mechanism.

Despite the interesting research prospects that the KGDP offers, it has hitherto not proved feasible to permanently reverse the injectivity declines. Partially for this reason and also because the geothermal plant cannot (at present) economically compete with other heat sources to a district heating scheme, the KGDP indefinitely ceased operation in 2017.

Data Availability

The data used to support the findings of this study are available from the corresponding author upon request.

Conflicts of Interest

The authors declare that they have no conflicts of interest.

Acknowledgments

The authors acknowledge the continuous support of the Geothermal Energy Systems team at Helmholtz-Zentrum Potsdam - Deutsches GeoForschungsZentrum GFZ and GTN-Neubrandenburg. The authors thank Geoterma for permission to publish this paper and the support during site visits. The DESTRESS project has received funding from the

European Union's Horizon 2020 research and innovation program under Grant Agreement no. 691728 and approved to publish this article. AJB is funded via the support of UK Natural Environment Research Council (NERC) for the Isotope Community Support Facility (*ICSF*) at SUERC.

References

[1] A. Grigelis, "Geology of Lithuania (Lietuva)," *Geological Survey of Norway Special Publication*, vol. 10, pp. 51–55, 2007.

[2] V. Juodkazis, P. Suveizdis, and V. Rastenienė, "Geothermal and mineral water resources of Lithuania," in *Mineral and Thermal Groundwater Resources*, pp. 281–316, Springer, 1997.

[3] B. Paukštys, "Groundwater in the crystalline basement of Lithuania," in *Hydrogeology of Hard Rocks, Memoirs of the XXIV Congress of International Association of Hydrogeologists, 28 June-2 July 1993*, pp. 1067–1074, Ås (Oslo), Norway, 1993.

[4] P. Suveizdis, V. Rasteniene, and V. Zui, "Geothermal field of the Vydmantai-1 borehole within the Baltic heat flow anomaly," *Baltica*, vol. 10, pp. 38–46, 1997.

[5] P. Suveizdis and V. Rastenienė, "The geothermal resources in Lithuania," *Lietuvos Geoterminiai*, vol. 4, p. 25, 1993.

[6] F. Zinevicius and S. Sliaupa, "Lithuania – geothermal energy country update," in *Proceedings World Geothermal Congress, 25-29th April 2010. Paper 0153*, pp. 1–7, Bali, Indonesia, 2010.

[7] B. Radeckas and V. Lukosevicius, "Klaipeda Geothermal Demonstration Project," in *Proceedings World Geothermal Congress, May 28 - June 10, 2000*, pp. 3547–3550, Kyushu – Tohoko, Japan, 2000.

[8] F. Zinevicius, A. Bickus, V. Rastenienė, and P. Suveizdis, "Inauguration of first geothermal plant in Lithuania," *International Geothermal Association (IGA) News*, vol. 59, pp. 4–6, 2005.

[9] M. Wolfgramm, A. Seibt, and K. Nowak, *Investigations into Injection Problems in Sandstone Aquifers*, Geothermie Neubrandenburg GmbH (GTN), Neubrandenburg, Germany, 2010.

[10] F. Zinevicius, V. Rastenienė, and A. Bickus, "Geothermal development in Lithuania," in *Proceedings of European Geothermal Conference*, pp. 25–30, Szeged, Hungary, 2003.

[11] M. Brehme, S. Regenspurg, P. Leary et al., "Injection-triggered occlusion of flow pathways in geothermal operations," *Geofluids*, vol. 2018, Article ID 4694829, 14 pages, 2018.

[12] PGI, *Klaipeda Geothermal Demonstration Project, Construction of Geothermal Wells. Well KGDP-2P, Final Well Report. World Bank loan IBRD 4013-LT*, Petroleum Geology Investigators ApS, 1998.

[13] PGI, *Klaipeda Geothermal Demonstration Project, Construction of Geothermal Wells. Well KGDP-3P, Final Well Report. World Bank Loan IBRD 4013-LT*, Petroleum Geology Investigators ApS, 1998.

[14] PGI, *Klaipeda Geothermal Demonstration Project, Construction of Geothermal Wells. Well KGCP-1I, Final Well Report. World Bank Loan IBRD 4013-LT*, Petroleum Geology Investigators ApS, 1998.

[15] PGI, *Klaipeda Geothermal Demonstration Project, Construction of Geothermal Wells. Well KGDP-4I, Final Well Report. World Bank Loan IBRD 4013-LT*, Petroleum Geology Investigators ApS, 1999.

[16] M. Wolfgramm and S. Sliaupa, *Investigations into the Injection Problems of the Klaipeda Geothermal Plant (Lithuania)*, Geothermie Neubrandenburg GmbH (GTN), 2008.

[17] C. Gerber, R. Vaikmäe, W. Aeschbach et al., "Using ^{81}Kr and noble gases to characterize and date groundwater and brines in the Baltic Artesian Basin on the one-million-year timescale," *Geochimica et Cosmochimica Acta*, vol. 205, pp. 187–210, 2017.

[18] Lenntech, *Major Ion Composition of Seawater*, Lenntech Water Treatment Solutions Website, 2018.

[19] Stanford University, *Mineral Makeup of Seawater*, Stanford University, California Website, 2018.

[20] IAEA/WMO, *Global Network of Isotopes in Precipitation*, The GNIP Database, IAEA/WMO, 2018.

[21] R. Mokrik, V. Juodkazis, A. Štuopis, and J. Mažeika, "Isotope geochemistry and modelling of the multi-aquifer system in the eastern part of Lithuania," *Hydrogeology Journal*, vol. 22, no. 4, pp. 925–941, 2014.

[22] R. Mokrik, J. Mažeika, A. Baublytė, and T. Martma, "The groundwater age in the Middle–Upper Devonian aquifer system, Lithuania," *Hydrogeology Journal*, vol. 17, no. 4, pp. 871–889, 2009.

[23] A. Babre, A. Kalvāns, K. Popovs et al., "Pleistocene age paleo-groundwater inferred from water-stable isotope values in the central part of the Baltic Artesian Basin," *Isotopes in Environmental and Health Studies*, vol. 52, no. 6, pp. 706–725, 2016.

[24] A. Paytan, E. T. Gray, Z. Ma, A. Erhardt, and K. Faul, "Application of sulphur isotopes for stratigraphic correlation," *Isotopes in Environmental and Health Studies*, vol. 48, no. 1, pp. 195–206, 2012.

[25] S. N. Davis, D. O. Whittemore, and J. Fabryka-Martin, "Uses of chloride/bromide ratios in studies of potable water," *Ground Water*, vol. 36, no. 2, pp. 338–350, 1998.

[26] A. Dickson and C. Goyet, "Handbook of methods for the analysis of the various parameters of the carbon dioxide system in sea water; version 2," Report No. ORNL/CDIAC-74, U.S. Department of Energy, 1994.

[27] D. Banks, *A Hydrogeological Atlas of Faryab Province, Northern Afghanistan*, NORPLAN, 2014.

[28] M. Brehme, K. Bauer, M. Nukman, and S. Regenspurg, "Self--organizing maps in geothermal exploration – a new approach for understanding geochemical processes and fluid evolution," *Journal of Volcanology and Geothermal Research*, vol. 336, pp. 19–32, 2017.

[29] D. Parkhurst and C. Appelo, "Description of input and examples for PHREEQC version 3—a computer program for speciation, batch-reaction, one-dimensional transport, and inverse geochemical calculations," in *U.S. Geological Survey Techniques and Methods, Book 6, Chap. A43*, p. 497, United States Geological Survey (USGS), 2013.

[30] K. S. Pitzer, "Thermodynamics of electrolytes. I. Theoretical basis and general equations," *Journal of Physical Chemistry*, vol. 77, no. 2, pp. 268–277, 1973.

[31] L. Plummer, D. Parkhurst, G. Fleming, and S. Dunkle, "A computer program incorporating Pitzer's equations for calculation of geochemical reactions in brines," in *U.S. Geological Survey Water-Resources Investigations Report 88-4153*, United States Geological Survey, 1988.

[32] M. B. Tomson, A. T. Kan, and J. E. Oddo, "Acid/base and metal complex solution chemistry of the polyphosphonate

DTPMP versus temperature and ionic strength," *Langmuir*, vol. 10, no. 5, pp. 1442–1449, 1994.

[33] HERA, *Human and Environmental Risk Assessment on Ingredients of European Household Cleaning Products*, HERA Project, Brussels, Belgium, 2004, Phosphonates (CAS 6419-19-8; 2809-21-4; 15827-60-8) - draft.

[34] B. Nowack, "Environmental chemistry of phosphonates," *Water Research*, vol. 37, no. 11, pp. 2533–2546, 2003.

[35] A. T. Kan, J. E. Oddo, and M. B. Tomson, "Formation of two calcium diethylenetriaminepentakis(methylene phosphonic acid) precipitates and their physical chemical properties," *Langmuir*, vol. 10, no. 5, pp. 1450–1455, 1994.

[36] P. Zhang, D. Shen, G. Ruan, A. T. Kan, and M. B. Tomson, "Mechanistic understanding of calcium–phosphonate solid dissolution and scale inhibitor return behavior in oilfield reservoir: formation of middle phase," *Physical Chemistry Chemical Physics*, vol. 18, no. 31, pp. 21458–21468, 2016.

[37] F. H. Browning and H. S. Fogler, "Fundamental study of the dissolution of calcium phosphonates from porous media," *AIChE Journal*, vol. 42, no. 10, pp. 2883–2896, 1996.

[38] J. Wang, Z. Y. Wang, and W. Ke, "Corrosion behaviour of weathering steel in diluted Qinghai salt lake water in a laboratory accelerated test that involved cyclic wet/dry conditions," *Materials Chemistry and Physics*, vol. 124, no. 2-3, pp. 952–958, 2010.